Effects of low molecular weight organic acids on the immobilization of aqueous Pb(II) using phosphate rock and different crystallized hydroxyapatite

ARTICLE *in* CHEMOSPHERE · NOVEMBER 2013

Impact Factor: 3.34 · DOI: 10.1016/j.chemosphere.2013.09.121 · Source: PubMed

3 AUTHORS, INCLUDING:

Wei Wei
Nanjing Normal University
22 PUBLICATIONS **150** CITATIONS
SEE PROFILE

Wei Zhenggui
University of Tasmania
47 PUBLICATIONS **840** CITATIONS
SEE PROFILE

Chemosphere 105 (2014) 14–23

Contents lists available at ScienceDirect

Chemosphere

journal homepage: www.elsevier.com/locate/chemosphere

Effects of low molecular weight organic acids on the immobilization of aqueous Pb(II) using phosphate rock and different crystallized hydroxyapatite

Wei Wei, Jing Cui, Zhenggui Wei *

Department of Environmental Science and Engineering, Nanjing Normal University, Nanjing 210023, PR China

HIGHLIGHTS

- Malic and citric acids could inhibit immobilization of Pb(II) by PR and HAp1.
- Oxalic acid enhanced the immobilization of Pb(II) by PR via precipitation with lead.
- Oxalic acid enhanced the dissolution of HAp1 by complexation with calcium.
- HAp2 had best immobilization efficiency of Pb regardless of the addition of LMWOAs.

ARTICLE INFO

Article history:
Received 10 August 2013
Received in revised form 25 September 2013
Accepted 27 September 2013
Available online 8 November 2013

Keywords:
Pb(II)
Immobilization
Poorly crystallized HAp
Oxalic acid
Malic acid
Citric acid

ABSTRACT

Understanding the effects of low molecular weight organic acids (LMWOAs) on the transformation of Pb(II) to geochemically stable pyromorphite (PY) by apatite materials (AMs), has considerable benefits for risk assessment and remediation strategies for contaminated water and soil. In this study, we systematically investigated the immobilization of Pb(II) from aqueous solution by natural phosphate rock (PR) and different crystallized hydroxyapatite (HAp) in the absence and presence of LMWOAs (oxalic, malic and citric acids). The results indicated that the effectiveness of PR and HAp in immobilizing Pb(II) followed in descending order by HAp2 (the poorly crystallized HAp), HAp1 (the well crystallized HAp) and PR, regardless of the presence of LMWOAs. The presence of malic and citric acids significantly decreased the immobilization efficiency of Pb(II) by HAp1 and PR, clarifying the lower adsorption affinities of Pb(II)-organic acid complexes on HAp1 and PR rather than Pb(II) ion. On the contrary, oxalic acid could markedly enhance the removal of Pb(II) from aqueous solution by HAp1 and PR through the formation of lead oxalate, which was confirmed by FT-IR and XRD analysis. Results also showed that LMWOAs had little promoting or inhibiting effect on the immobilization of Pb(II) by HAp2. This study suggested that the ubiquity of LMWOAs in natural environments could retard the transformation efficiency of Pb(II) to PY by AMs, especially in the presence of oxalic acid, and the poorly crystallized HAp2 had great potential to remediate Pb(II)-contaminated water and soil due to its insusceptibility to LMWOAs.

1. Introduction

Contamination of heavy metals in the environment is of major concern because of their toxicity and threat to human life and the environment. Pb(II) is one of the most toxic heavy metals in waste water, largely released from non-ferrous metallurgy and lead acid battery manufacture (Zhang et al., 2012). Pb(II) can enter human body directly through respiratory system, digestive system or skin and cause damages to nearly every organ, especially it can be accumulated in the brain and severely impact on the children's intelligence development (Ryan et al., 2004). Therefore, the removal of Pb(II) from aqueous solution or contaminated soil has attracted considerable attention.

In recent years, the use of apatite materials (AMs) for the adsorption and immobilization of heavy metals has been considered as a promising pollution control technology, due to the low cost, high efficiency, easy-to-implement, and environmental-friendly nature (Zhang et al., 2010; Jiang et al., 2012; Liu and Zhao, 2013). It has been reported that AMs such as hydroxyapatite [HAp, $Ca_{10}(PO_4)_6(OH)_2$] and phosphate rock [PR, primarily $Ca_{10}(PO_4)_6F_2$] could significantly reduce Pb, Cd, Cu, and Zn availability through the formation of metal phosphates (Cao et al., 2009; Stötzel et al., 2009; Chen et al., 2010), while minimizing soil acidification and potential risk of eutrophication associated with the application of highly soluble phosphate sources (Mignardi et al., 2012).

* Corresponding author. Tel./fax: +86 8439 5014.
E-mail addresses: weizhenggui@gmail.com, zgwei@njnu.edu.cn (Z. Wei).

0045-6535/$ - see front matter © 2013 Elsevier Ltd. All rights reserved.
http://dx.doi.org/10.1016/j.chemosphere.2013.09.121

Moreover, several studies also showed that the immobilization efficiency and selectivity of AMs for Pb(II) were much higher than that of other heavy metals (Smičiklas et al., 2008; Chen et al., 2010; Mobasherpour et al., 2012). Therefore, researchers have paid much attention to Pb(II) immobilization by various AMs and achieved significant results in the immobilization mechanism and influencing factors.

The dominant reaction mechanism for Pb(II) immobilization by AMs has been reported to be through apatite dissolution and subsequent precipitation of sparingly soluble pyromorphite [PY, $Pb_{10}(PO_4)_6(OH, Cl, F)_2$] like minerals, though mechanisms such as cation substitution, adsorption and precipitation as other Pb(II) minerals are also possible (Ma, 1996; Mavropoulos et al., 2002; Cao et al., 2004). Based on the dissolution–precipitation mechanism, parameters affecting apatite dissolution, PY precipitation, and especially soluble P concentration, will affect Pb(II) immobilization by AMs. Factors influencing the effectiveness of Pb(II) immobilization include pH, coexisting ions, dissolved organic matter, as well as the physical and chemical properties of AMs. It is generally accepted that inducing soil acidic conditions will promote the transformation of Pb(II) to insoluble phosphate (Cao et al., 2009). On one hand this is due to acidic condition facilitates the dissolution of Pb(II) compounds and release of Pb^{2+} from contaminated soil and sediment. On the other hand, acidic condition promotes the liberation of P from AMs and enhances the formation of PY. In addition, when AMs are used for Pb(II) immobilization, the coexisting cations can compete for P by formation metal phosphates, which would retard the immobilization efficiency of Pb(II). For example, researchers (Ma et al., 1994a,b) have studied the effects of aqueous cations and anions on Pb(II) immobilization by HAp, and found that metal ions inhibited Pb(II) immobilization by HAp in the order: A1 > Cu > Fe(II) > Cd > Zn > Ni, and Cu > Fe(II) > Cd > A1 > Ni at high and low initial Pb(II) concentrations, respectively. On the contrary, NO_3^- and SO_4^{2-} anions did not have any effects on HAp effectiveness, while large cocentrations of CO_3^{2-} resulted in some what poorer Pb(II) removal (Ma et al., 1994a). However, chloropyromorphite and fluoropyromorphite precipitated after the reaction of HAp with aqueous Pb(II) in the presence of Cl^- and F^- ions. Moreover, the presence of high amounts of soil organic matter (SOM) was reported to inhibit the synthesis of PY due to the formation of chelates and SOM coatings on PY seed crystals that prevent further precipitation of PY (Lang and Kaupenjohann, 2003). Furthermore, the physical and chemical properties of AMs such as particle size, specific surface area, crystallinity, and isomorphous substitution, had significant effects on the immobilization of Pb(II). Several studies (Chen et al., 2006; Hashimoto and Sato, 2007; Stötzel et al., 2009) suggested that the decrease in crystallinity or particle size of AMs led to an increase in specific surface area, accompanied by a concomitant rise in the quantity of active sites on the surface, which would cause a remarkable enhancement of Pb(II) immobilization. Similar findings were reported by Giammar et al. (2008) who suggested that the biogenic apatite has a high degree of carbonate substitution for phosphate, which contributed to a decrease in crystallinity and an increase in solubility, and thus the carbonated apatite exhibited better immobilization efficiency for Pb(II) than synthetic HAp.

However, despite many investigations on the factors influencing the immobilization of Pb(II) by AMs (Ma, 1996; Smičiklas et al., 2008), knowledge of the influence of low molecular weight organic acids (LMWOAs) on the adsorption and immobilization of Pb(II) by AMs is still limited. LMWOAs (mainly oxalic, malic and citric acids) widely occur in water and soil as natural products of root exudates, microbial metabolism, and decomposition of plant and animal residues (Li et al., 2006). The LMWOAs possessing one or more carboxyl and hydroxyl groups can form complexes with metals and thus play an important role in mineral weathering, nutrient acquisition and metal detoxification (Jones et al., 2003). On one hand, the use of chelating agents and LMWOAs in phytoremediation of metal-contaminated soils was known to increase the availability of metals to plants (Wu et al., 2003, 2004) and thus might enhance the formation of PY. In fact, Hettiarachchi et al. (2001) have suggested that acetic acid addition to Pb(II) contaminated soil significantly reduced the bioavailability of Pb(II) as determined by the physiologically based extraction test. On the other hand, the hindering effects of organic acids on the adsorption of Cu (II) onto HAp were firstly reported by Wang et al. (2009). In addition, Debela et al. (2010, 2013) have recently indicated that the addition of oxalic and citric acids could inhibit the formation of PY in P-amended contaminated soil. However, little knowledge is available about the effects and mechanisms of LMWOAs on the removal of Pb(II) from aqueous solution. Information concerning the influencing mechanisms of LMWOAs on the immobilization of Pb(II) by different crystallized HAp is even more deficient.

The objectives of this work are to investigate the immobilization of aqueous Pb(II) by HAp with different degrees of crystallinity, and study the effects and mechanisms of LMWOAs on immobilization of Pb(II) by HAp and PR. Data from FT-IR spectroscopy and powder XRD are used to provide an understanding of the influencing mechanisms of LMWOAs on the immobilization of Pb(II) by HAp and PR. The knowledge obtained may be of great importance in understanding the effects of crystallinity and organic acid binding on the immobilization of Pb(II) by AMs.

2. Materials and methods

2.1. Materials

PR was purchased from Taizhou Changpu Chemical Reagent Company (China), and used without further purification. Oxalic, malic, and citric acids, obtained from Shanghai Guoyao Chemical Reagent Company (China), were used in the study as representative LMWOAs. For the preparation of different crystallized HAp, $Ca(NO_3)_2{\cdot}4H_2O$, $NH_4H_2PO_4$, $(NH_4)_2$-EDTA, $NH_3{\cdot}H_2O$, $CaCO_3$, and H_3PO_4 were purchased from Nanjing Chemical Reagent Company (China). $Pb(NO_3)_2$, $NaNO_3$ and 2-(N-morpholino) ethanesulfonic acid were obtained from Shanghai Chemical Reagent Factory (China). All the chemicals were of analytical grade. Deionized water was purified by Millipore Milli-Q system.

2.2. Preparation of different crystallized HAp

The well crystallized HAp (noted HAp1) used in this study was prepared by the thermal decomposition of precursors, this method was described in detail in our previous work (Wei et al., 2010). Briefly, Appropriate amounts of $Ca(NO_3)_2{\cdot}4H_2O$, $(NH_4)_2$-EDTA, and $NH_4H_2PO_4$ aqueous solutions were mixed together at a molar ratio of EDTA:Ca:P = 2.667:1.667:1, and stirred until a homogeneous solution was formed approximately for 5 min. The final pH of the solution was controlled to 5–6 by the addition of ammonia solution. After slowly evaporating the solvent, the precursors were obtained and then were dried at 80 °C. The dried precursors were calcined at 800 °C for 4 h in air to obtain well crystallized HAp.

The poorly crystallized HAp (noted HAp2) was prepared by a neutralization method described by Li (2009) with a little modification. This method was considered to be an effective route to obtain HAp nanocrystals with lower crystallinity, smaller size, and greater surface area (Smičiklas et al., 2005). Generally, calcium oxide (obtained by calcination of $CaCO_3$ at 1100 °C) was suspended in distilled water, and a required amount of H_3PO_4 was added until the end point is reached (pH = 7.0). After the complete addition, the suspension was further stirred for 2 h and centrifuged at

4000 rpm for 10 min. Then the precipitated HAp was washed with deionized water till the pH turned to 7.0. The resultant powders were dried at 80 °C for 24 h, and then calcined at 100 °C for 1 h to obtain poorly crystallized HAp.

2.3. Characterization of PR and HAp

Several methods were used to characterize PR and different crystallized HAp. FT-IR analysis was applied to determine the surface functional groups, by using a FT-IR spectroscope (Tensor 27, Bruker, Germany), where the spectra were recorded from 4000 to 400 cm^{-1}. The phase purity and crystallinity of PR and HAp were determined by powder XRD using Cu Kα (λ = 1.5405 Å) radiation on a Rigaku D/max-IIIB X-ray powder diffractometer (Tokyo, Japan). The morphology and size of the PR and HAp were characterized by a Hitachi Model H-7650 transmission electron microscope (TEM) (Tokyo, Japan) and a Hitachi Model S-3000N scanning electron microscope (SEM) (Tokyo, Japan).

The specific surface area of PR and HAp were determined by nitrogen adsorption at 77 K (Micromeritics ASAP 2010, USA). Surface area was calculated from adsorption data using BET equation. The point of zero charge (pH_{PZC}) was determined by the batch equilibrium technique (Chutia et al., 2009). For this, 0.1 g of each sample was treated with 40 mL 0.1 M KNO_3 solution which was used as an inert electrolyte. The initial pH values ($pH_{initial}$) were adjusted in the range ~2.4 to ~11.24 by adding minimum amounts of 0.1 M KOH or 0.1 M HNO_3 solutions. The suspensions were allowed to equilibrate for 24 h in a rotary shaker fixed at 180 rpm at room temperature. After completion of the equilibration time, the admixtures were filtered and final pH values (pH_{final}) of the filtrates were measured again. The pH_{PZC} values were obtained from the plateau parts of the pH_{final} versus $pH_{initial}$ plots.

2.4. Adsorption experiments

Adsorption experiments were conducted in batch equilibrium mode. All experiments were conducted by mixing 40 mL of aqueous Pb(II) solutions with 0.1 g of the different adsorbents in the absence and presence of LMWOAs (oxalic acid, malic acid, and citric acid). Effect of pH was studied over the range of 2.0–10.0 and pH adjustments were made by the addition of dilute aqueous solutions of HNO_3 and NaOH. The ionic strength was adjusted to 0.01 M using $NaNO_3$. Sodium nitrate was chosen as background electrolyte because Na^+ ions, especially at lower concentration, had little competition with heavy metals for the adsorption sites of minerals or soils (Hatter and Naidu, 2001). The mixtures were shaken at room temperature for 12 h. After shaking time was completed, the suspension was centrifuged at 5000 rpm for 10 min, and Pb(II) concentrations in the solutions were then determined by atomic absorption spectrometry (Varian AA 240 FS, USA). The adsorption capacity were calculated from the difference between the initial and final concentrations of Pb(II) in the solutions. The experiments were performed in triplicate and mean values were taken into account. The solid residues loaded with Pb(II) were washed with deioned water, air dryed and analyzed by FT-IR and XRD.

3. Results and discussion

3.1. Properties of PR and HAp

The surface area of PR, HAp1, and HAp2 measured by the BET method were determined to be 18, 42, and 72 $m^2\ g^{-1}$, respectively. The pH_{PZC} is a concept related to the phenomenon of adsorption that describes the condition when the electrical charge density on the adsorbent surface is zero. The pH_{PZC} were found to be 7.5, 7.9, and 6.2, for PR, HAp1, and HAp2, respectively. (Fig. SM-1 in Supplementary Material (SM)).

Fig. 1a showed the FT-IR spectra of the PR and synthetic HAp samples. The vibrational bands of phosphate and adsorbed water were observed in all the samples. The absorption peaks located at 1090 and 1045 cm^{-1} originated from asymmetrical stretching (v_3) of PO_4^{3-} and at 571 and 602 cm^{-1} were attributed to bending modes (v_4) of PO_4^{3-}. While the symmetric stretching modes (v_1 and v_2) of PO_4^{3-} were also observed at around 962 and 472 cm^{-1} (Wei et al., 2009). In addition, the broad bands at 1630 and 3447 cm^{-1} were attributed to adsorbed water (Nayar et al., 2006). In particular, bands at 3572 and 632 cm^{-1}, corresponding to the stretching and bending vibrational modes of the OH^- groups, respectively, were evidenced for HAp. As expected, the spectrum of PR did not show these peaks. Moreover, in the case of PR sample, the peaks at 1458 and 1433 cm^{-1} were attributed to the anti-symmetrical elastic vibrating v_3 absorption patterns of CO_3^{2-} in PR; and 885 and 727 cm^{-1} were the elastic vibrating v_2 and v_4 absorption patterns of CO_3^{2-}, respectively (Bianco et al., 2010). The locations of these bands indicated presence of predominantly type-B (carbonate substituted for phosphate) carbonated apatite in PR sample. Furthermore, some CO_2-derived bands were

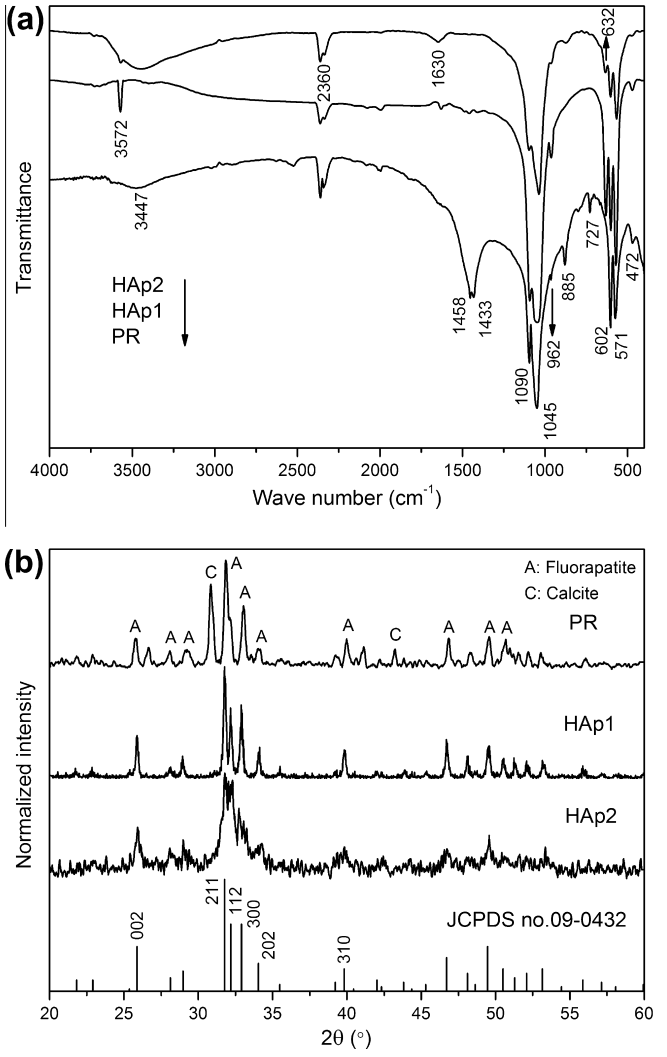

Fig. 1. (a) The FT-IR spectra of PR and the synthetic HAp samples and (b) The XRD patterns of PR, the synthetic HAp samples and the reference pattern of pure HAp (JCPDS No. 09-0432).

observed around 2360 cm^{-1}. It might be due to the adsorption of atmospheric carbon dioxide during the sample preparation. These results agreed with the literature data by other researchers (Comodi and Liu, 2000; Antonakos et al., 2007).

The XRD analyses (Fig. 1b) indicated that the synthetic HAp samples were in good agreement with the reference pattern of pure hydroxyapatite (JCPDS No. 09-0432). However, the degrees of crystallinity of HAp1 and HAp2 were different. For HAp1 (obtained by a thermal decomposition of precursors at 800 °C), many sharp peaks appeared, suggesting that the sample was well crystallized. By contrast, the HAp2 sample (prepared by a neutralization method and calcined at 100 °C) showed comparatively low crystallinity. From XRD data, the fraction of the crystalline phase (X_c) in HAp samples could be determined as: $X_c = 1-(V_{112/300}/I_{300})$, where $V_{112/300}$ represented the intensity of the hollow between diffraction peaks (112) and (300), and I_{300} was the intensity of (300) diffraction peak (Stötzel et al., 2009). The degree of crystallinity determined in this study was 0.87 and 0.32 for HAp1 and HAp2, respectively. The average particle size (D) of the synthetic HAp samples could be calculated from the XRD line broadening measurement from the Scherrer formula (Sanosh et al., 2009). The average particle size of HAp1 and HAp2 were 59 and 29 nm, respectively.

The XRD analysis of PR indicated that the main minerals in PR structure were fluorapatite (JCPDS No. 15-0876) and calcite (JCPDS No. 15-0876), which were similar with the results reported by Jiang et al. (2012). The diffraction pattern produced by fluorapatite phase in PR was similar to that of HAp, due to the fact that fluoride substitution for hydroxyl did not significantly affect the diffraction pattern. However, there was a slight shift of the (300) peak to the right-hand side in the PR which indicated the substitution of OH with F ions in the fluorapatite structure. Similar findings were reported by Montazeri et al. (2010) who suggested that the (300) reflections from HAp and fluorapatite occurred at 2θ angles of 32.86° and 33.12°, respectively. This shift has been related to the a-axis contraction caused by smaller size of F ions compared to OH ions. Another point to note was the presence of sharper peaks in the XRD patterns of PR. This feature might be due to increased crystallinity of PR as compared to synthetic HAp.

TEM micrographs (Fig. 2) showed that the HAp was irregular and needle like particles for HAp1 and HAp2, respectively. According to the micrographs, the particle size could also be estimated. The average particle size of HAp1 and HAp2 were 60 and 30 nm, respectively, which were consistent with the XRD results. Moreover, it is worth noting that HAp2 presents a much better dispersed morphology than HAp1.

The surface structure of PR was analyzed by SEM (Fig. 2). This figure revealed that the PR particles were mostly irregular in shape and seemed to be non-porous. While it was seen that the particle-size distribution was not continuous, relatively large particles were mixed with a much finer size.

3.2. Immobilization of Pb(II) by PR and HAp in the absence of LMWOAs

Fig. 3a showed the effect of pH on the adsorption and immobilization of Pb(II) by PR and different crystallized HAp. It was clear to see that the adsorption capacity of Pb(II) decreased continuously with increasing pH for all the three adsorbents, and Pb(II) was adsorbed poorly at pH > 6.0. The maximal adsorption capacity of Pb(II) on PR, HAp1 and HAp2 were at pH 2.0, and the adsorption capacities were 129 (64% removal), 164 (82% removal) and 199 mg g^{-1} (99% removal), for PR, HAp1 and HAp2, respectively. While at pH 10.0, the adsorption capacities of Pb(II) decreased to 51 (26% removal), 66 (33% removal), and 126 (63% removal) mg g^{-1}, for PR, HAp1 and HAp2, respectively. Our results corresponded to Xu and Schwartz (1994) who reported that Pb(II)

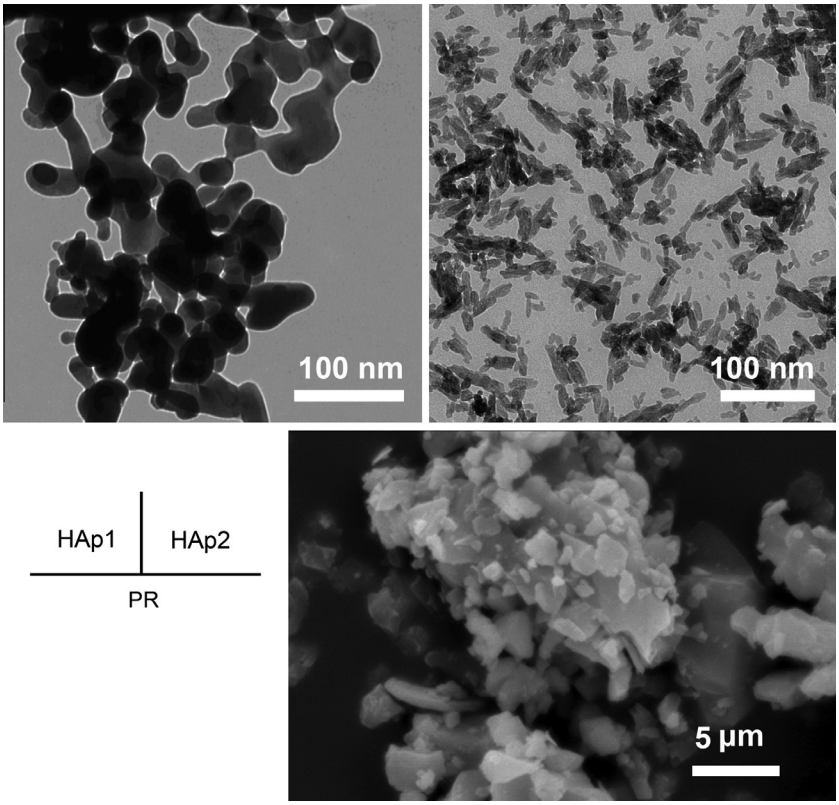

Fig. 2. The TEM micrograph of the synthetic HAp samples and the SEM micrograph of PR.

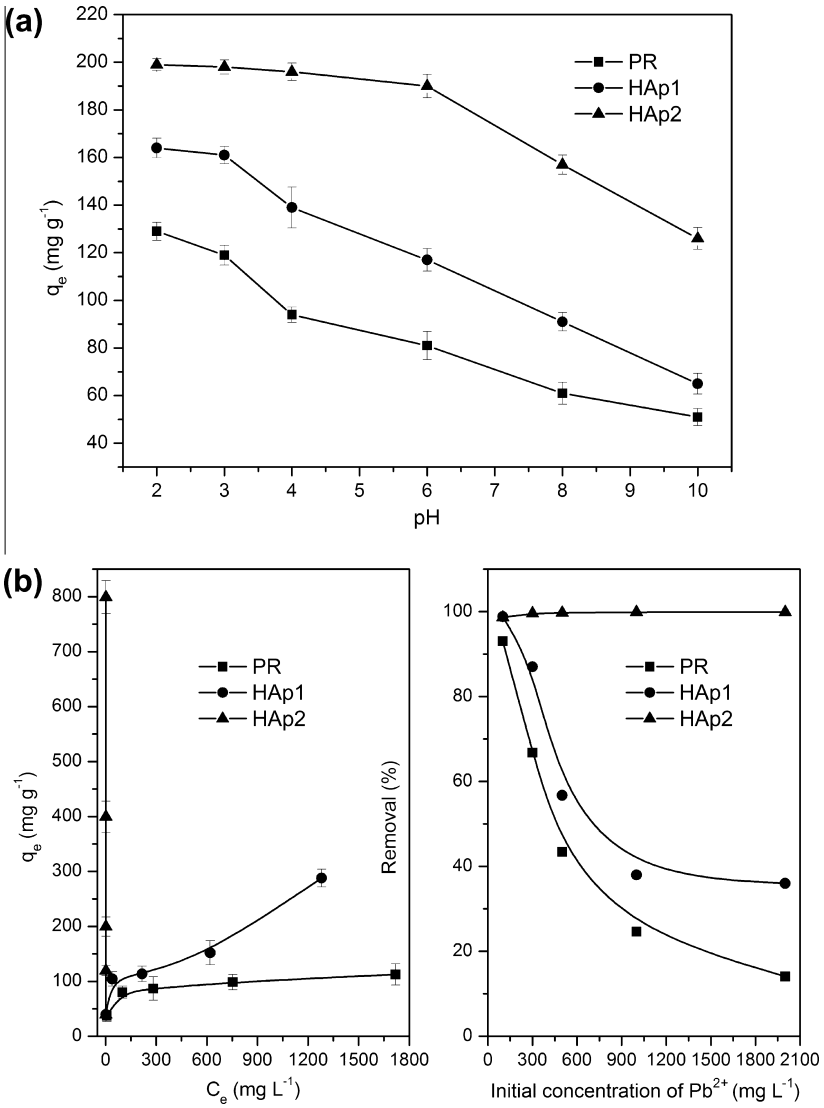

Fig. 3. (a) Effect of pH on the adsorption of Pb(II) by PR and different crystallized HAp. (adsorbent dosage = 0.1 g, initial Pb^{2+} concentration = 500 mg L^{-1}, initial pH = 4.0, contact time 12 h) and (b) The adsorption isotherms of Pb(II) on the well crystallized HAp1, the poorly crystallized HAp2 and PR. (adsorbent dosage = 0.1 g, temperature = 298 K, initial pH = 4.0, contact time 12 h).

removal by HAp was maximized in the acidic solution, which was due to the primary mechanism for Pb(II) removal by AMs was based on the reaction that dissolution of AMs liberated phosphate for the subsequent precipitation of Pb(II) as PY.

The adsorption isotherms of Pb(II) on the well crystallized HAp1, the poorly crystallized HAp2 and PR were presented in Fig. 3b, which showed that the quantities of Pb(II) adsorbed against the final Pb(II) concentration in equilibrium solutions. It was clear from Fig. 3b that the adsorption capacity of Pb(II) by HAp2 increased linearly with the equilibrium concentration, which not only indicated a high affinity between Pb(II) and the HAp2 surface, but also suggested that the adsorption sites on HAp2 were sufficient and the amount of adsorption in the studied concentration range was dependent on the number of Pb(II) that was transported from the bulk solution to the surfaces of adsorbent. In the case of HAp1 and PR, the experimental adsorption isotherms data were compared with the Langmuir and the Freundlich isotherm models. The adsorption data were better fitted to the Freundlich isotherm since the correlation coefficients for the Freundlich isotherm were higher than that for the Langmuir isotherm (Table SM-1).

The results in Fig. 3b also showed that the adsorption capacity of HAp2 for Pb(II) was much higher than that of HAp1 and PR. For instance, when the initial concentration of Pb(II) was 1000 mg L^{-1}, the adsorption capacity was 399, 152 and 98 mg g^{-1} for HAp2, HAp1 and PR, respectively. Moreover, within the concentration range investigated, the removal efficiency of Pb(II) by HAp2 was constantly above 99%, while that by HAp1 and PR decreased significantly with an increase in the concentration of Pb(II). As far as PR, HAp1 and HAp2 were concerned, it should be pointed out that the notable differences among them were the crystallinity and particle size of PR and HAp1 were larger than HAp2. And it was generally considered that the well crystallized HAp had stronger structures than the poorly crystallized HAp (Oazaki et al., 1982), which would lead to a higher solubility of HAp2 than PR and HAp1. Similar results obtained in our previous work (Wei et al., 2011) suggesting that the poorly crystallized HAp could release more Ca and P than the well crystallized HAp. Therefore, based on the dissolution–precipitation mechanism, the adsorption and immobilization efficiency of Pb(II) decreased in the following order: HAp2 > HAp1 > PR.

3.3. Effects of LMWOAs on the Immobilization of Pb(II) by PR and HAp

Fig. 4a showed the effects of 5 mM of oxalic, malic and citric acids on the adsorption and immobilization of Pb(II) (100–2000 mg L^{-1}) by PR and different crystallized HAp. Results indicated that oxalic acid could significantly enhance the adsorption of Pb(II) by PR and HAp1. When the concentration of Pb(II) changed from 100 to 2000 mg L^{-1} at a oxalic acid concentration of 5 mM, the adsorption of Pb(II) by PR increased markedly from 37–113 to 39–419 mg g^{-1}. Mean while, compared to the control, the adsorption of Pb(II) by HAp1 increased from 39–343 to 40–96 mg g^{-1} in the presence of 5 mM oxalic acid. Similar results were also proposed by Jiang et al. (2012), who have reported that oxalic acid treatment could significantly enhance the immobilization efficiency of Pb(II) by PR. In particular, Elliott and Herzig (1999) have ever indicated that oxalic acid could form insoluble lead oxalate ($K_{sp} = 2.74 \times 10^{-11}$) with Pb(II) in contaminated soil. The present results suggested that the presence of oxalic acid could enhance the removal of Pb(II) from aqueous solution through precipitation of lead oxalate, which has been confirmed by XRD analyses. On the other hand, in our previous work (Wei et al., 2011), it was shown that the adsorption capacity of oxalic acid on HAp was much higher than malic and citric acids, so oxalic acid adsorption would significantly increase the negative surface charges of HAp other than malic and citric acids, the increase in the negative surface charge by adsorbing oxalic acid promoted the adsorption of Pb(II) by PR and HAp. Nevertheless, the adsorption of Pb(II) by PR and HAp1 could be significantly inhibited by malic and citric acids. As shown in Fig. 4a, the inhibiting effect of malic acid on the adsorption of Pb(II) by PR was much higher than that of citric acid. But for HAp1 and HAp2, citric acid inhibited the adsorption of Pb(II) to a greater extent than that of malic acid. This was probably due to the different adsorption ability of malic and citric acids on PR and HAp. Similarly, The inhibiting effect of LMWOAs on the adsorption of metal ions by HAp were reported by Wang et al. (2009), who suggested that the presence of organic acids (formalic acid, succinic acid, citric acid, acetic acid, oxalic acid, tartaric acid and EDTA) significantly decreased the adsorption quantity of Cu(II) by nanosized HAp, clarifying the lower sorption affinities of Cu(II)-organic acid complexes onto the HAp rather than Cu(II) ion. By contrast, it should be noted that oxalic acid inhibited the remove of Cu(II) while promoted the remove of Pb(II). This was mainly due to the fact that oxalic acid and Pb(II) produced precipitation, while oxalic acid and Cu(II) resulted in water-soluble complex. Moreover, the adsorption of Pb(II) by poorly crystallized HAp2 was less affected by LMWOAs, since the removal efficiency of Pb(II) (100–1000 mg L^{-1}) by HAp2 was constantly above 98% in the presence of 5 mM of oxalic, malic or citric acid.

In order to further investigate the effects of LMWOAs on the adsorption of Pb(II) by PR and different crystallized HAp, the adsorption experiments were performed in the presence of different concentrations of LMWOAs, and the results were shown in Fig. 4b. When the concentration of oxalic acid changed from 0 to 10 mM at a Pb(II) concentration of 1000 mg L^{-1}, the adsorption of Pb(II) by PR and HAp1 increased significantly from 96 to 397 and 150 to 394 mg g^{-1}, respectively. When the concentration of oxalic acid increased to 20 mM, the adsorption of Pb(II) increased minimally from 397 to 399 mg g^{-1} and 394 to 396 mg g^{-1}, respectively. In contrary, the adsorption of Pb(II) by PR and HAp1 decreased continually with increasing malic and citric acids concentration. These results were different from that reported by Huang et al. (2010), who suggested that low LMWOAs (acetic acid, tartaric acid and citric acid) concentrations (<0.6 or 1.0 mM) promoted Pb(II) adsorption by goethite and montmorillonite, while high LMWOAs concentrations (>1.0 mM) inhibited Pb(II) adsorption. Different Pb(II) adsorption reaction mechanism between clay minerals and AMs might be responsible for the aforementioned results. As Pb(II) was adsorbed and immobilized by AMs through a dissolution–precipitation mechanism, but the adsorption of Pb(II) by clay minerals was mainly via electrostatic attraction.

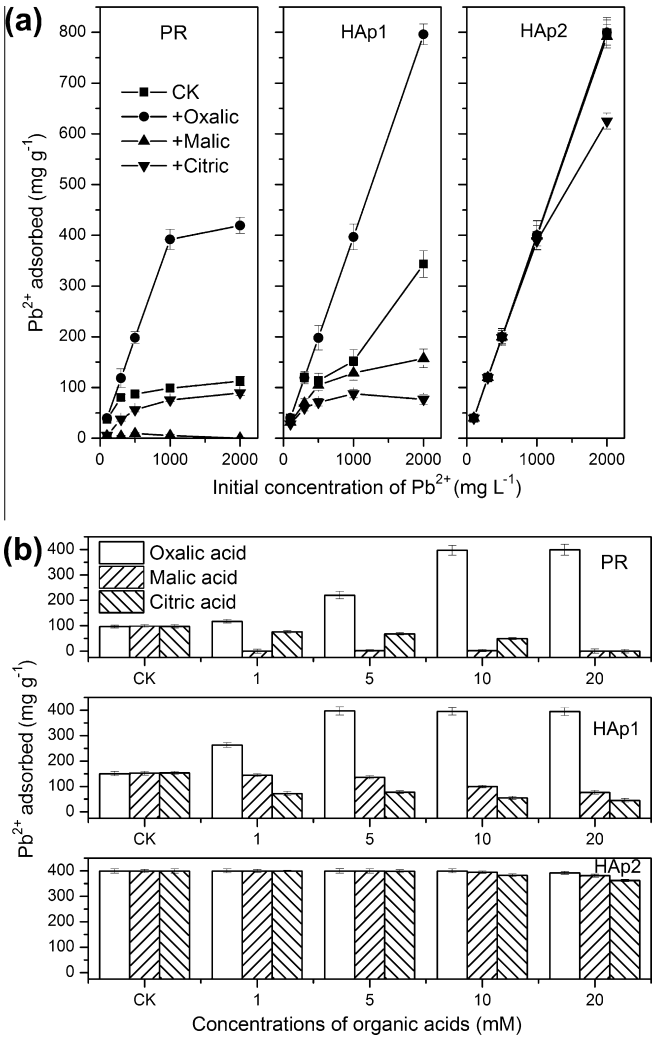

Fig. 4. (a) Efects of oxalic, malic and citric acids on the immobilization of different concentrations of Pb(II) by PR, HAp1 and HAp2. (adsorbent dosage = 0.1 g, concentration of each organic acid = 5.0 mM, initial pH = 4.0, contact time 12 h) and (b) Effects of different concentrations of oxalic, malic and citric acids on the immobilization of Pb(II) by PR, HAp1 and HAp2. (adsorbent dosage = 0.1 g, initial concentration of Pb^{2+} = 1000 mg L^{-1}, initial pH = 4.0, contact time 12 h).

Based on the above results, it could draw the conclusion that the LMWOAs (malic and citric acids) might depress Pb(II) adsorption by PR and HAp1 via the formation of stable aqueous non-adsorbing metal–organic acid complexes. Moreover, the poor adsorption of malic and citric acids by PR and HAp (Wei et al., 2011) were not conductive to the adsorption of of Pb(II) through electrostatic attraction. Conversely, oxalic acid might increase the Pb(II) adsorption through electrostatic attraction, formation of Pb(II)-oxalic acid-surface complex and/or surface precipitation, due to the strong adsorption of oxalic acid by HAp (Yoshida et al., 2001; Welch et al., 2002). On the other hand, Pb(II) could also be removed by precipitation as lead oxalate. It must be pointed out that the adsorption of Pb(II) by poorly crystallized HAp2 in the presence of LMWOAs was constantly high regardless of the added concentrations of LMWOAs. The excellent Pb(II) adsorption performance of HAp2 was mainly dependent on its special properties. Compared to HAp1 and PR, HAp2 had much poorer crystallinity,

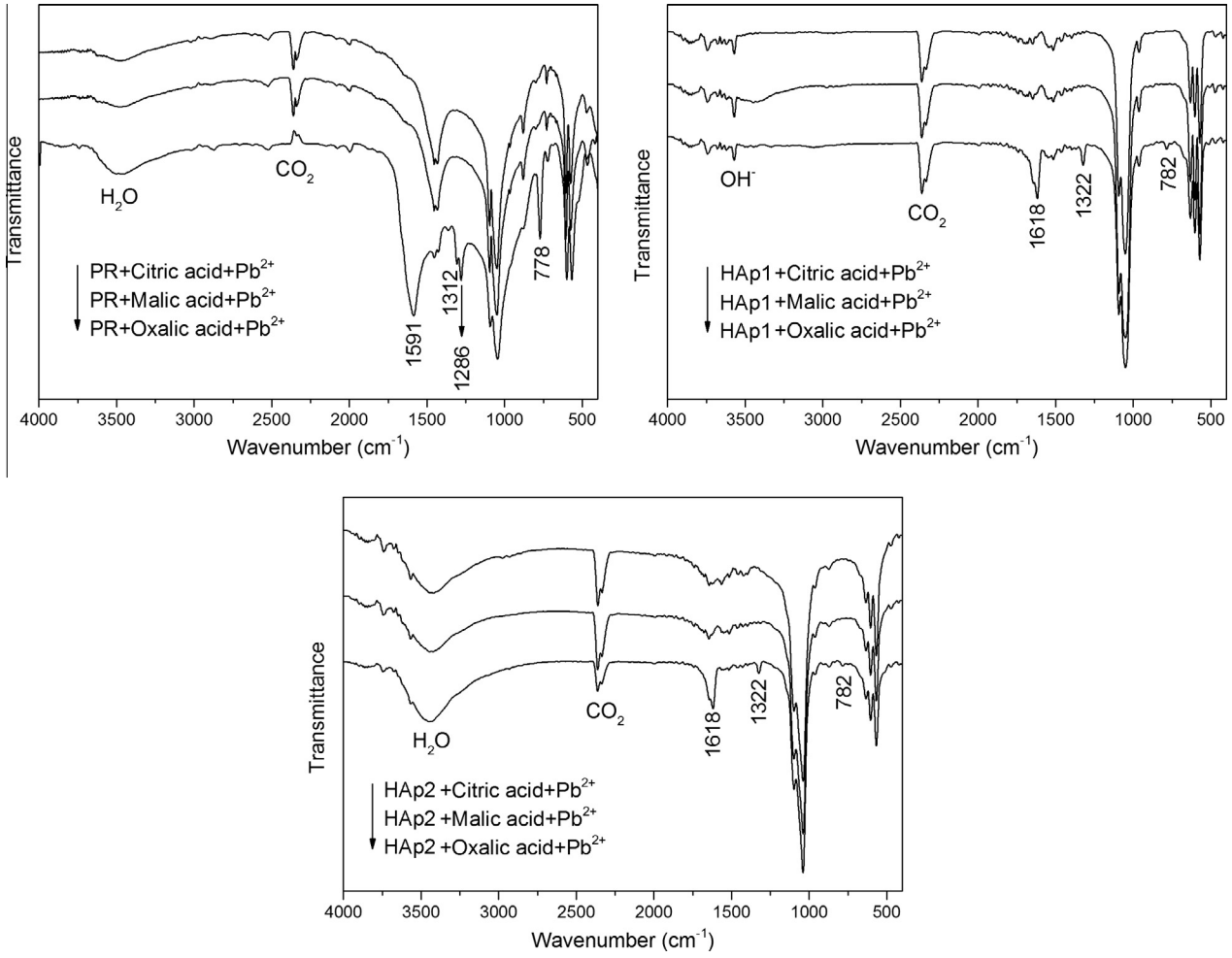

Fig. 5. The FT-IR spectra of PR, well crystallized HAp1 and poorly crystallized HAp2 after adsorption of Pb(II) in the presence of 5 mM LMWOAs. (adsorbent dosage = 0.1 g, initial concentration of Pb^{2+} = 1000 mg L^{-1}, initial pH = 4.0, contact time 12 h).

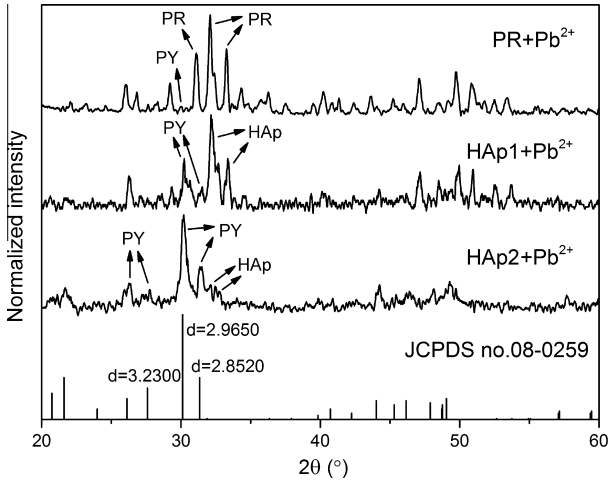

Fig. 6. The XRD patterns of PR, HAp1, and HAp2 after adsorption of Pb(II) in the absence of LMWOAs. (adsorbent dosage = 0.1 g, initial concentration of Pb^{2+} = 1000 mg L^{-1}, initial pH = 4.0, contact time 12 h).

better dispersed morphology and smaller particle size, which made the adsorption capacity of HAp2 much higher than PR and HAp1, and the adsorption of Pb(II) by poorly crystallized HAp2 was less affected by LMWOAs due to its high reaction activity.

3.4. Infrared spectra analyses

The FT-IR spectra of PR, well crystallized HAp1 and poorly crystallized HAp2 after adsorption of Pb(II) in the presence of 5 mM LMWOAs were shown in Fig. 5. The results demonstrated that there were no significant differences between the FT-IR spectra of PR, HAp1, HAp2 before (Fig. 1a) and after (Fig. 5) adsorption of Pb(II) in the presence of 5 mM citric or malic acid. This was not only due to the fact that citric or malic acid could form water-soluble Pb(II)-organic acid complexes, which had lower adsorption affinities to PR, HAp1, and HAp2, but also due to the poor adsorption of citric or malic acid by PR, HAp1, and HAp2.

In the case of oxalic acid, the FT-IR spectra of PR, HAp1, and HAp2 after adsorption of Pb(II) in the presence of 5 mM oxalic acid exhibited strong absorptions for the $C_2O_4^{2-}$ in the asymmetric and symmetric vibration regions. The main antisymmetric carbonyl stretching band ν_{as} (COO^-) specific to the lead oxalate occurred at 1591 cm^{-1}, and the secondary carbonyl stretching band, the metal-carboxylate stretches, ν_s (COO^-), were located at 1312 and 1286 cm^{-1} (Mancilla et al., 2009). The infrared bands observed at 778 and 510 cm^{-1} could be assigned to the O—C=O out-of-plane bending mode and in-plane bending mode of oxalate, respectively (Behnoudnia and Dehghani, 2012). All of these bands for PR after adsorption of Pb(II) in the presence of 5 mM oxalic acid corresponded to the FT-IR spectra of lead oxalate reported by Mancilla et al. (2009). Thus it could be inferred that oxalic acid could

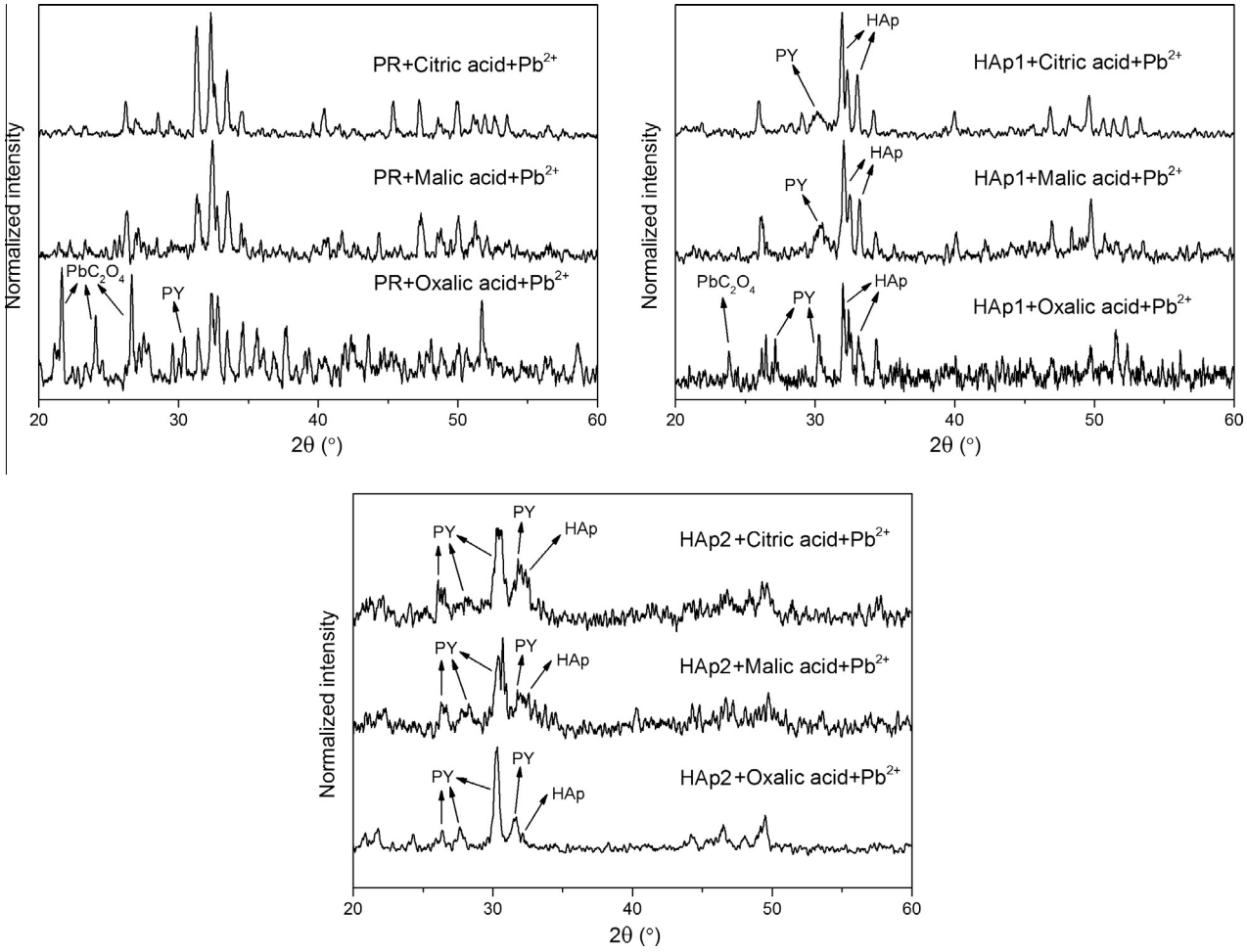

Fig. 7. The XRD patterns of PR, HAp1, and HAp2 after adsorption of Pb(II) in the presence of LMWOAs. (adsorbent dosage = 0.1 g, initial concentration of Pb^{2+} = 1000 mg L^{-1}, initial pH = 4.0, contact time 12 h).

precipitate with Pb(II) on the PR surface and promoted the removal of Pb(II) from aqueous solution. As for HAp1 and HAp2, the FT-IR spectrum exhibited strong absorptions for the carbonyls of the oxalate carboxylate ligands in the asymmetric and symmetric vibration regions. Specifically, asymmetric stretching vibrations ν_{as} (COO^-) appeared at 1618 cm^{-1} (with a weak shoulder in its higher energy side, 1645 cm^{-1}), whereas the symmetric ones $\nu_s(COO^-)$ were observed at 1322 cm^{-1} (Ouyang et al., 2003). The peak at 782 cm^{-1} belonged to the out-of-plane bending band of water. All of the bands were shifted to lower frequencies compared to the free oxalic acid, denoting the changes in the vibrational status of that ligand upon complexation to calcium. The aforementioned assignments were in agreement with previously examined complexes of oxalate with calcium (Deng et al., 2006). These results indicated that the adsorption and immobilization of Pb(II) by HAp1 and HAp2 in the presence of oxalic acid were mainly through formation of PY rather than the precipitation of lead oxalate. However, the structure changes of PR, HAp1, and HAp2 after adsorption of Pb(II) in the presence of LMWOAs should be further studied.

3.5. XRD analyses

Fig. 6 showed the XRD patterns of PR, HAp1, and HAp2 after adsorption of Pb(II) in the absence of LMWOAs. It was shown that no structural changes of PR were detected by XRD analysis of the solid residue, obtained after interaction of PR with 1000 mg L^{-1} Pb(II). This result was consistent with the poor immobilization efficiency of Pb(II) by PR. As for HAp1 and HAp2, PY phase could be identified obviously by comparison of the diffraction patterns of JCPDS database (pyromorphite, JCPDS No. 08-0259) (Harris and Lottermoser, 2006). In particular, XRD result indicated that the poorly crystallized HAp2 almost completely converted to PY, which suggested that the immobilization efficiency of Pb(II) by HAp2 was much higher than that of PR and HAp1.

The XRD patterns of PR, HAp1, and HAp2 after adsorption of Pb(II) in the presence of 5 mM LMWOAs are shown in Fig. 7. In the case of PR, it was demonstrated that there were no significant differences between the XRD patterns of PR before (Fig. 1B) and after (Fig. 7) adsorption of Pb(II) in the presence of 5 mM citric or malic acid, due to the inhibiting effects of citric and malic acids on the immobilization of Pb(II) by PR. By contrast, lead oxalate phase was confirmed in the XRD pattern of PR after adsorption of Pb(II) in the presence of 5 mM oxalic acid, and in this case only a small amount of PY could be observed. This might be attributed to the fact that oxalic acid could enhance the immobilization of aqueous Pb(II) through precipitation as lead oxalate rather than the formation of PY.

As for HAp1, citric and malic acids could significantly inhibited its immobilization efficiency for Pb(II), due to the formation of water-soluble Pb(II)-organic acid complexes, thus only a small amount of PY could be observed in the XRD patterns (Fig. 7). And it was considered that oxalic acid could enhance the immobilization efficiency of Pb(II) by HAp1, due to the strong complexation of oxalic acid with calcium on HAp1 surface, as indicated by FT-IR spectra and our previous work (Wei et al., 2011). This complex-

ation could promote the dissolution of HAp1 and accordingly enhance the immobilization of Pb(II) through formation of PY, based on the dissolution–precipitation mechanism.

In the case of poorly crystallized HAp2, the immobilization of Pb(II) by HAp2 was not affected by LMWOAs, since HAp2 completely converted to PY despite the presence of citric, malic, or oxalic acid as indicated by the XRD patterns in Fig. 7. And there was no other mineral phase, such as lead oxalate could be observed in the XRD pattern. Considering that the geochemical stability of PY was much higher than lead oxalate, it was generally accepted that aqueous Pb(II) should be transformed to sparingly soluble PY rather than lead oxalate. Based on the above results, it was suggested that The poorly crystallized HAp2 had great potential in the immobilization of Pb(II).

4. Conclusions

This study showed that the immobilization efficiencies of Pb(II) by PR and different crystallized HAp were of the following sequence: the poorly crystallized HAp2 > the well crystallized HAp1 > PR. Malic and citric acids could significantly inhibit the immobilization of aqueous Pb(II) by PR and the well crystallized HAp1, due to the formation of water-soluble non-adsorbing Pb(II)-organic acid complexes. Oxalic acid could enhance the immobilization of Pb(II) by PR through precipitation of lead oxalate, while the promoting effect of oxalic acid on the immobilization of Pb(II) by the well crystallized HAp1 was suggested to be achieved via the strong complexation of oxalic acid with calcium on HAp1 surface, which enhanced the dissolution of HAp1 and the transformation of Pb(II) to PY. By contrast, the poorly crystallized HAp2 had much poorer crystallinity, better dispersed morphology and smaller particle size than PR and HAp1, and thus was less susceptible to LMWOAs. The immobilization efficiency of Pb(II) by HAp2 was much higher than PR and HAp1 regardless of the presence of LMWOAs. These results indicated that the poorly crystallized HAp2 might be a promising adsorbent for the immobilization of Pb(II) from aqueous solutions.

Acknowledgments

This work is supported by the National Natural Science Foundation of China (No. 41303081), the National Programs for High Technology Research and Development of China (No. 2007AA10Z406), the Program of Natural Science Research of Jiangsu Higher Education Institutions of China (No. 12KJB610002), the Foundation for Talent Recommendation Program of Nanjing Normal University (No. 2009103XGQ0063 and No. 2011105XGQ0247), the Research Fund for the Doctoral Program of Higher Education (No. 20113207110014 and 20133207120019), SRF for ROCS, SEM, and PAPD (a project funded by the Priority Academic Program Development of Jiangsu Higher Education Institutions).

Appendix A. Supplementary material

Supplementary data associated with this article can be found, in the online version, at http://dx.doi.org/10.1016/j.chemosphere.2013.09.121.

References

Antonakos, A., Liarokapis, E., Leventouri, T., 2007. Micro-Raman and FTIR studies of synthetic and natural apatites. Biomaterials 28, 3043–3054.
Behnoudnia, F., Dehghani, H., 2012. Synthesis and characterization of novel three-dimensional-cauliflower-like nanostructure of lead(II) oxalate and its thermal decomposition for preparation of PbO. Inorg. Chem. Commun. 24, 32–39.
Bianco, A., Cacciotti, I., Lombardi, M., Montanaro, L., Bemporad, E., Sebastiani, M., 2010. F-substituted hydroxyapatite nanopowders: thermal stability, sintering behaviour and mechanical properties. Ceram. Int. 36, 313–322.
Cao, X.D., Ma, L.Q., Rhue, D.R., Appel, C.S., 2004. Mechanisms of lead, copper, and zinc retention by phosphate rock. Environ. Pollut. 131, 435–444.
Cao, X.D., Wahbi, A., Ma, L., Li, B., Yang, Y.L., 2009. Immobilization of Zn, Cu, and Pb in contaminated soils using phosphate rock and phosphoric acid. J. Hazard. Mater. 64, 555–564.
Chen, S.B., Ma, Y.B., Chen, L., Xian, K., 2010. Adsorption of aqueous Cd^{2+}, Pb^{2+}, Cu^{2+} ions by nano-hydroxyapatite: single- and multi-metal competitive adsorption study. Geochem. J. 44, 233–239.
Chen, S.B., Zhu, Y.G., Ma, Y.B., 2006. The effect of grain size of rock phosphate amendment on metal immobilization in contaminated soils. J. Hazard. Mater. 30, 74–79.
Chutia, P., Kato, S., Kojima, T., Satokawa, S., 2009. Arsenic adsorption from aqueous solution on synthetic zeolites. J. Hazard. Mater. 162, 440–447.
Comodi, P., Liu, Y., 2000. CO_3 substitution in apatite further insight from new crystal-chemical data of Kasekere (Uganda) apatite. Eur. J. Min. 12, 965–974.
Debela, F., Arocena, J.M., Thring, R.W., Whitcombe, T., 2010. Organic acid-induced release of lead from pyromorphite and its relevance to reclamation of Pb-contaminated soils. Chemosphere 80, 450–456.
Debela, F., Arocena, J.M., Thring, R.W., Whitcombe, T., 2013. Organic acids inhibit the formation of pyromorphite and Zn-phosphate in phosphorous amended Pb- and Zn-contaminated soil. J. Environ. Manage. 116, 156–162.
Deng, S.P., Zheng, H., Ouyang, J.M., 2006. Crystallization rules of calcium oxalate crystals in lithogenic urine and in healthy urine in vitro. Mater. Sci. Eng. C 26, 683–687.
Elliott, H.A., Herzig, L.M., 1999. Oxalate extraction of Pb and Zn from polluted soils: Solubility limitations. J. Soil Contam. 8, 105–116.
Giammar, D.E., Xie, L.Y., Pasteris, J.D., 2008. Immobilization of lead with nanocrystalline carbonated apatite present in fish bone. Environ. Eng. Sci. 25, 725–735.
Harris, D.L., Lottermoser, B.G., 2006. Phosphate stabilization of polyminerallic mine wastes. Mineral. Mag. 70, 1–13.
Hashimoto, Y., Sato, T., 2007. Removal of aqueous lead by poorly-crystalline hydroxyapatites. Chemosphere 69, 1775–1782.
Hatter, R.D., Naidu, R., 2001. An assessment of environmental and solution parameter impact on trace-metal sorption by soils. Soil Sci. Soc. Am. J. 65, 597–612.
Hettiarachchi, G.M., Pierzynski, G.M., Ransom, M.D., 2001. In situ stabilization of soil lead using phosphorus. J. Environ. Qual. 30, 1214–1221.
Huang, L., Hu, H.Q., Li, X.Y., Li, L.Y., 2010. Influences of low molar mass organic acids on the adsorption of Cd^{2+} and Pb^{2+} by goethite and montmorillonite. Appl. Clay Sci. 49, 281–287.
Jiang, G.J., Liu, Y.H., Huang, L., Fu, Q.L., Deng, Y.J., Hu, H.Q., 2012. Mechanism of lead immobilization by oxalic acid-activated phosphate rocks. J. Environ. Sci. 24, 919–925.
Jones, D.L., Dennis, P.G., Owen, A.G., van Hees, P.A.W., 2003. Organic acid behavior in soils – misconceptions and knowledge gaps. Plant Soil 248, 31–41.
Lang, F., Kaupenjohann, M., 2003. Effect of dissolved organic matter on the precipitation and mobility of the lead compound chloropyromorphite in solution. Eur. J. Soil Sci. 54, 139–148.
Li, C.F., 2009. The crystallinity of calcium phosphate powders influenced by the conditions of neutralized procedure with citric acid additions. Mater. Res. Bull. 44, 1136–1141.
Li, J., Xu, R., Tiwari, D., Ji, G., 2006. Effect of low-molecular-weight organic acids on the distribution of mobilized Al between soil solution and solid phase. Appl. Geochem. 21, 1750–1759.
Liu, R.Q., Zhao, D.Y., 2013. Synthesis and characterization of a new class of stabilized apatite nanoparticles and applying the particles to in situ Pb immobilization in a fire-range soil. Chemosphere 91, 594–601.
Ma, L.Q., 1996. Factors influencing the effectiveness and stability of aqueous lead immobilization by hydroxyapatite. J. Environ. Qual. 25, 1420–1429.
Ma, Q.Y., Logan, T.J., Traina, S.J., Ryan, J.A., 1994a. Effects of NO_3^-, Cl^-, F^-, SO_4^{2-}, and CO_3^{2-} on Pb^{2+} immobilization by hydroxyapatite. Environ. Sci. Technol. 28, 408–418.
Ma, Q.Y., Traina, S.J., Logan, T.J., Ryan, J.A., 1994b. Effects of aqueous Al, Cd, Cu, Fe(II), Ni, and Zn on Pb immobilization by hydroxyapatite. Environ. Sci. Technol. 28, 1219–1228.
Mancilla, N., D'Antonio, M.C., González-Baró, A.C., Baran, E.J., 2009. Vibrational spectra of lead(II) oxalate. J. Raman Spectrosc. 40, 2050–2052.
Mavropoulos, E., Rossi, A.M., Costa, A.M., Perez, C.A.C., Moreira, J.C., Saldanha, M., 2002. Studies on the mechanisms of lead immobilization by hydroxyapatite. Environ. Sci. Technol. 36, 1625–1629.
Mignardi, S., Corami, A., Ferrini, V., 2012. Evaluation of the effectiveness of phosphate treatment for the remediation of mine waste soils contaminated with Cd, Cu, Pb, and Zn. Chemosphere 86, 354–360.
Mobasherpour, I., Salahi, E., Pazouki, M., 2012. Comparative of the removal of Pb^{2+}, Cd^{2+} and Ni^{2+} by nano crystallite hydroxyapatite from aqueous solutions: adsorption isotherm study. Arab. J. Chem. 5, 439–446.
Montazeri, L., Javadpour, J., Shokrgozar, M.A., Bonakdar, S., Javadian, S., 2010. Hydrothermal synthesis and characterization of hydroxyapatite and fluorhydroxyapatite nano-size powders. Biomed. Mater. 5, 1–8.
Nayar, S., Sinha, M.K., Basu, D., Sinha, A., 2006. Synthesis and sintering of biomimetic hydroxyapatite nanoparticles for biomedical applications. J. Mater. Sci. Mater. Med. 17, 1063–1068.

Oazaki, M., Takahashi, J., Kimura, H., 1982. Crystallinity, solubility and dissolution rate behavior of fluoridated CO3 apatites. J. Biomed. Mater. Res. 16, 851–860.
Ouyang, J.M., Duan, L., Tieke, B., 2003. Effects of carboxylic acids on the crystal growth of calcium oxalate nanoparticles in lecithin–water liposome systems. Langmuir 19, 8980–8985.
Ryan, J.A., Scheckel, K.G., Berti, W.R., Brown, S.L., Casteel, S.W., Chaney, R.L., Hallfrisch, J., Doolan, M., Grevatt, P., Maddaloni, M., Mosby, D., 2004. Reducing children's risk from lead in soil. Environ. Sci. Technol. 38, 18A–24A.
Sanosh, K.P., Chu, M.C., Balakrishnan, A., Lee, Y.J., Kim, T.N., Cho, S.J., 2009. Synthesis of nano hydroxyapatite powder that simulate teeth particle morphology and composition. Curr. Appl. Phys. 9, 1459–1462.
Smičiklas, I., Onjia, A., Raičević, S., 2005. Experimental design approach in the synthesis of hydroxyapatite by neutralization method. Sep. Purif. Technol. 44, 97–102.
Smičiklas, I., Onjia, A., Raičević, S., Janaćković, Đ., Mitrić, M., 2008. Factors influencing the removal of divalent cations by hydroxyapatite. J. Hazard. Mater. 152, 876–884.
Stötzel, C., Müller, F.A., Reinert, F., Niederdraenk, F., Barralet, J.E., Gbureck, U., 2009. Ion adsorption behaviour of hydroxyapatite with different crystallinities. Colloid. Surface B 74, 91–95.
Wang, Y.J., Chen, J.H., Cui, Y.X., Wang, S.Q., Zhou, D.M., 2009. Effects of low molecular weight organic acids on Cu(II) adsorption onto hydroxyapatite nanoparticles. J. Hazard. Mater. 162, 1135–1140.
Wei, W., Sun, R., Cui, J., Wei, Z.G., 2010. Removal of nitrobenzene from aqueous solution by adsorption on nanocrystalline hydroxyapatite. Desalination 263, 89–96.
Wei, W., Sun, R., Wei, Z.G., Zhao, H.Y., Li, H.X., Hu, F., 2009. Elimination of the interference from nitrate ions on oxalic acid in RP-HPLC by solid-phase extraction with nanosized hydroxyapatite. J. Liq. Chromatogr. Related Technol. 32, 106–124.
Wei, W., Zhang, X., Cui, J., Wei, Z.G., 2011. Interaction between low molecular weight organic acids and hydroxyapatite with different degrees of crystallinity. Colloid. Surface A 392, 67–75.
Wu, L.H., Luo, Y.M., Christie, P., Wong, M.H., 2003. Effects of EDTA and low molecular weight organic acids on soil solution properties of a heavy metal polluted soil. Chemosphere 50, 819–822.
Wu, L.H., Luo, Y.M., Xing, X.R., Christie, P., 2004. EDTA-enhanced phytoremediation of heavy metal contaminated soil with Indian mustard and associated potential leaching risk. Agric. Ecosyst. Environ. 102, 307–318.
Xu, Y., Schwartz, F.W., 1994. Lead immobilization by hydroxyapatite in aqueous solutions. J. Contam. Hydrol. 15, 187–206.
Zhang, F., Zhao, Z.S., Tan, R.Q., Xu, W., Jiang, G.B., Song, W.J., 2012. Efficient and selective immobilization of Pb^{2+} in highly acidic wastewater using strontium hydroxyapatite nanorods. Chem. Eng. J. 203, 110–114.
Zhang, Z.Z., Li, M.Y., Chen, W., Zhu, S.Z., Liu, N.N., Zhu, L.Y., 2010. Immobilization of lead and cadmium from aqueous solution and contaminated sediment using nano-hydroxyapatite. Environ. Pollut. 158, 514–519.